A. Macchi[1, 2], T. V. Liseykina[3], P. Londrillo[4], M. Passoni[5], A. Sgattoni[5, 1], M. Tamburini[1, 2] and A. Zani[5]

[1] *Istituto Nazionale di Ottica, CNR, research unità "A. Gozzini", Pisa* – [2] *Dipartimento di Fisica "E. Fermi", Università di Pisa* – [3] *Institut für Physik, Universität Rostock, Germany* – [4] *INAF, Osservatorio Astronomico di Bologna* – [5] *Dipartimento di Energia, Politecnico di Milano*

TOFUSEX

Towards Full-Scale Simulation of Laser-Plasma Experiments

Introduction

The aim of the TOFUSEX project was to perform large-scale simulations of laser-plasma interactions with Particle-In-Cell (PIC) codes, upgraded and optimized in order to improve the capability to design and interpret real experiments. Specific tasks were the improvement of performance and I/O management to enable three-dimensional (3D) simulations on very large number of processors, as well as the inclusion of additional physics, such as Radiation Reaction effects, for the investigation of forthcoming experiments at "extreme" intensities.

Two simulation codes, UMKA and ALaDyn, have been used during the project. UMKA and ALaDyn are both fully parallelized PIC codes, which effectively solve the system of (relativistic) kinetic equations for plasma electrons and ions, coupled with Maxwell's equations for the electromagnetic fields, using a discrete particle representation of the phase space. The two codes presently implement different algorithms making one or the other most suitable for specific problems.

In the following we present a short survey of results from two specific simulation campaigns, both focused on regimes of ion acceleration by superintense laser pulses [1]. The first campaign was devoted to simulations of radiation pressure acceleration (RPA) of thin foils at ultra-high intensities, addressing the role of both laser pulse polarization and Radiation Reaction (RR). The second campaign was oriented to a study of the interaction with low-density "foam" targets, of direct relevance for an experiment scheduled in 2012.

Polarization and Radiation Reaction Effects on Superintense Laser-Foil Interaction

The radiation pressure generated by ultraintense laser pulses may drive strong acceleration of dense matter and be an effective mechanism for the generation of high-energy ions, especially in the regime of extremely high intensities and relativistic ion energies as foreseen with the Extreme Light Infrastructure (ELI) European project. In the case of solid-density thin foil targets, earlier PIC simulations have shown that at intensities exceeding 10^{23} W cm^{-2} and for linear polarization (LP) of the laser pulse, radiation pressure eventually dominates the acceleration. This yields a linear scaling of the ion energy with the laser pulse intensity, high efficiency and quasi-monoenergetic features in the ion energy spectrum [2]. Other studies have shown that the use of Circular Polarization (CP) instead of LP and normal incidence quenches the generation of high-energy electrons [3] allowing radiation pressure to dominate even at lower intensities and leading to efficient acceleration of ultrathin foils [4, and references therein]. A systematic comparison of LP versus CP in the radiation pressure dominant acceleration (RPDA) regime where ions become relativistic has not been performed yet. Furthermore, it has been previously shown by 1D PIC simulations that Radiation Reaction (RR) effects may significantly affect the dynamics of radiation pressure acceleration and also depend strongly on the laser pulse polarization [5, and references therein]. To address these issues as well as other multi-dimensional effects (bending instabilities, anisotropies, conservation of angular momentum for CP light) we performed fully 3D simulations of the RPDA regime with RR effects included (for the first time in a 3D code). Details of the RR modeling and original numerical implementation are given in Refs. [5, 6].

We present a total of four 3D simulations each with the same physical and numerical parameters but different polarization, with and without RR effects. In these simulations, the laser field amplitude has a $\sin^2$-function longitudinal profile with 8λ FWHM (where $\lambda = 0.8$ m) is the laser wavelength) while the transverse radial profile is Gaussian with 10λ FWHM and the laser pulse front reaches the edge of the plasma foil at $t = 0$. The peak intensity is $I = 1.7\times10^{23}$, W cm^{-2} which corresponds to a normalized amplitude $a_0 = 280$ for LP and $a_0 = 198$ for CP. The target is a plasma foil of electrons and protons with uniform initial density $n_0 = 64n_c$ (where $n_c = \pi m_e c^2/e^2\lambda^2$ is the critical density), thickness $\ell = 1\lambda$ and initially located in the region $10\lambda \le x \le 11\lambda$. The simulation grid is $1320\times896\times896$. and the spatial step is λ44 for each direction. The timestep is $T/100$ where $T = \lambda/c = 2.67$ fs is the laser period. We use 216 particles per cell for each species and the total number of particles is 1.526×10^{10}. The runs were performed using 1024 processors of the IBM-SP6 cluster at the CINECA supercomputing facility in Bologna, Italy. Details on the results are reported in Ref. [7].

Fig.1 shows the ion and the electron 3D spatial distributions at $t = 20T$ for the LP case without (a) and with (b) RR and for the CP case without (c) and with (d) RR. The color corresponds to the range in kinetic energy. In the LP case the most energetic ions are grouped into two off-axis clumps lengthened and aligned along the polarization direction. RR effects are much stronger for LP, where the density and the total number of ions grouped into the highest energy populations is strongly enhanced in the case with RR as seen by the comparison

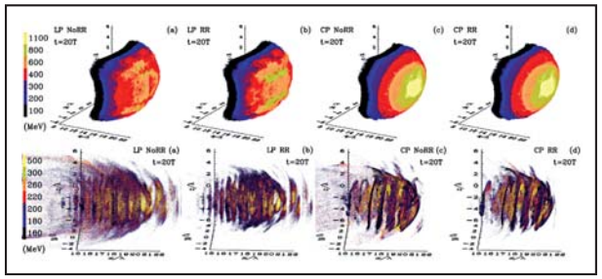

Fig. 1. – Spatial distributions of ions (upper row) and electrons (lower row) at $t = 20\,T$ and in the region $-5.7 \le (y, z)/\lambda \le 5.7$, for LP without (a) and with (b) RR and for CP without (c) and with (d) RR. Ions and electrons are divided into seven populations according to their kinetic energy, with the color-bar reporting the lower bound of the energy interval. In the LP case [frames (a),(b)], the polarization is along the y axis.

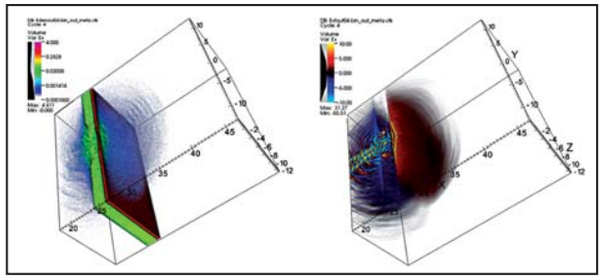

Fig. 2. – 3D simulation for a target constituted by a thin foil (0.5 m of Aluminium with $n_e = 40n_c$) and a foam layer (2 m C with $n_e = 2n_c$). The electron density in logarithmic colour scale (left) and the longitudinal electric field (right) are shown at $t = 66$ fs. Half of the simulation space has been removed for easier viewing.

of Figs.1 (a) and (b); on the contrary, RR plays a minor role for CP affecting only a small fraction of ultra-relativistic electrons with almost no influence on the ion distribution which has rotational symmetry around the central axis and a distribution in energy monotonically decreasing with increasing radial distance, as seen in Fig. 2, frames (c), (d). The electron spatial distribution has an helicoidal shape with spatial step $\sim \lambda$ Fig.2 (c), (d).

The differences between CP and LP can be explained by the absence of the oscillating component of the $\mathbf{J}\times\mathbf{B}$ force for CP [3]. Thus, in the CP case we have a steady push of the foil with weak penetration of the laser pulse in the plasma. Most of the electrons move coherently with the foil and in the same direction as the laser pulse so that the RR force may also become very small [2, 5]. For LP pulses, the longitudinal oscillations driven by the 2 component of the $\mathbf{J}\times\mathbf{B}$ cause the electrons to collide with the counterpropagating laser pulse twice per cycle [5]. Our 3D results confirm the strong differences between CP and LP also for a focused laser pulse and a strongly bent target.

Interaction with low-density foam-layered targets

In current experiments, the laser-plasma acceleration of protons is typically achieved focusing a high power laser pulse (10-500TW) on thin solid targets 0.1÷10 m). Since the electron density $n_e > nc$ the laser -penetrates only in the thin skin layer, of depth $\sim c\omega_p = (\lambda/2\pi)(n_c/n_e)^{1/2}$, and is partially reflected by the surface. However, a considerable part of the laser pulse energy is absorbed into high-energy electrons. These latter can cross the target and escape from its rear side towards vacuum. The charge separation hence created builds an electrostatic field which accelerates the protons present on the surface of the target. This is the basis of the so-called Target Normal Sheath Acceleration (TNSA) acceleration regime [1]. The efficiency of this process strongly depends on the fraction of energy

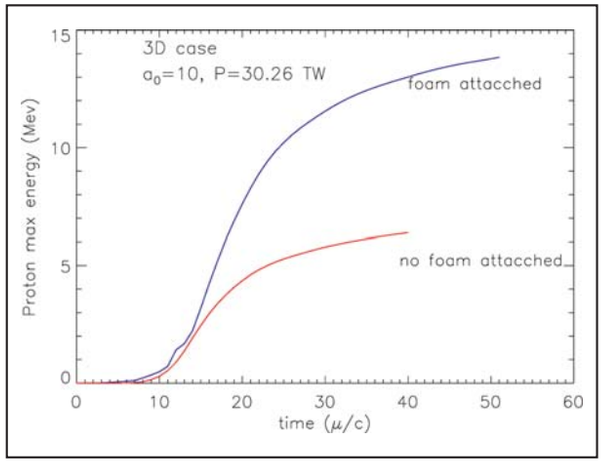

Fig. 3. – Proton maximum energy evolution with respect to time in 3D PIC simulations.

of the laser pulse absorbed by the electrons. The absorption increases for decreasing values of the plasma density. Hence, plasmas with $n_e \simeq n_c$ are expected to lead to a high absorption [8, 9, 10] but such a condition is difficult to explore experimentally because targets with such a "near-critical" density are not easy to fabricate. Within the FIRB project SULDIS the "nanolab" group at Politecnico di Milano is currently producing nano-structured target with low density foams deposited on metal surfaces which will be soon used in experiments. The aim of our numerical investigation has been to understand the physics of the interaction of the laser with a near-critical plasma and to estimate the proton energies which can be obtained in the future experiments with such targets.

We explored this configuration with several 2D and 3D simulations using the code ALaDyn. In the context of TNSA the 3D geometry is essential in order to quantitatively reproduce the dynamics of the expansion of the electron cloud around the target. 3D simulations of the laser interaction with highly over-dense plasmas, as is the case of these targets where the near critical density plasma is coupled with a solid foil, are very demanding in terms of number of grid points. A grid cell size smaller the skin-depth ($\simeq 10^{-2}\lambda = 10$ nm is needed and a high number of macro-particles per cell is essential to represent the sharp density gradients of the plasma. Our 3D runs were performed on 1024 and 2048 cores of the SP6 machine. The simulation grid was $1880\times1024\times1024$ and grid step was $\lambda/100$.

The laser pulse has $w_0 = 3$ m, $\tau = 25$ fs and $a_0 = 10$ being respectively the pulse waist, time duration and normalized vector potential, corresponding to a pulse with a peak power of 32 TW and intensity $I = 2\times10^{20}$ W/cm^2. Fig. 3 represents the electron density in presence of a foam and the longitudinal electric field which accelerates the protons present on the rear side (right) of the target. Fig. 3 represents the evolution of the maximum proton energy with respect to time for the two configurations: with and without foam layer. Although the foam layer considered is rather thin (2 m) it leads to an increase of the proton energy by a factor of nearly 3. The 2D simulation support these results and allow for a broader parameter investigation confirming how a suitably constructed target may lead to a much improved laser-to-target energy transfer and higher proton energy. This configuration will be investigated experimentally at the beginning of 2012. Meanwhile, the 2D code has also been validated by the comparison with experimental parametric studies of TNSA acceleration [11].

Acknowledgement

This work was sponsored by the Italian Ministry of University and Research via the FIRB project "SULDIS". We acknowledge the CINECA Award N.HP10A25JKT-2010 under the ISCRA initiative, for the availability of high performance computing resources and support.

Bibliography

(1) A. Macchi, M. Borghesi and M. Passoni, *Rev. Mod. Phys.*, to be published 2011.
(2) T. Esirkepov, M. Borghesi, S. V. Bulanov, G. Mourou and T. Tajima, *Phys. Rev. Lett.* **92**, 175003, 2004.
(3) A. Macchi, F. Cattani, T. V. Liseykina and F. Cornolti, *Phys. Rev. Lett.*, **94**, 165003, 2005.
(4) A. Macchi, S. Veghini and F. Pegoraro, *Phys. Rev. Lett. 103*, 085003, 2009.
(5) M. Tamburini, F. Pegoraro, A. Di Piazza, C. H. Keitel and A. Macchi, *New J. Phys.*, **12**, 123005, 2010.
(6) M. Tamburini, *Nucl. Inst. Meth. Phys. Res. A*, **653**, 181, 2011.
(7) M. Tamburini, T. V. Liseykina, F. Pegoraro and A. Macchi, *ArXiv e-prints*, 1108.2372, 2011.
(8) L. Willingale, *Phys. Rev. Lett.* **102**, 125002, 2009.
(9) S. S. Bulanov, *Physics of Plasmas*, **17**, 043105, 2010.
(10) T. Nakamura, M. Tampo, R. Kodama, S. V. Bulanov and M. Kando, *Physics of Plasmas*, **17**, 113107, 2010.
(11) A. Zani, A. Sgattoni and M. Passoni, *Nucl. Inst. Meth. Phys. Res. A*, **653**, 94, 2011.